Wang, Xiaojia and Jin, Baosheng and Zhu, Xiaoming and Liu, Hao (2016) Experimental evaluation of a novel 20kWth in situ gasification chemical looping combustion unit with an iron ore as the oxygen carrier. Industrial and Engineering Chemisty Research, 55 (45). pp. 11775-11784. ISSN 0888-5885

I&EC research
Industrial & Engineering Chemistry Research

Article

pubs.acs.org/IECR

Experimental Evaluation of a Novel 20 kW_{th} in Situ Gasification Chemical Looping Combustion Unit with an Iron Ore as the Oxygen Carrier

Xiaojia Wang,[†] Baosheng Jin,[*,†] Xiaoming Zhu,[†] and Hao Liu[*,‡]

[†]Key Laboratory of Energy Thermal Conversion and Control of Ministry of Education, School of Energy & Environment, Southeast University, Nanjing 210096, People's Republic of China

[‡]Faculty of Engineering, University of Nottingham, Nottingham NG7 2RD, U.K.

Supporting Information

ABSTRACT: This study presents the results obtained from the operation of a 20 kW_{th} in situ gasification chemical-looping combustion (iG-CLC) unit with a Chinese bituminous coal as the fuel and a natural iron ore as the oxygen carrier. This unit was built based upon the concept of a novel iG-CLC system evaluated through our previous cold-model tests. It is mainly composed of a high-flux circulating fluidized bed riser as the fuel reactor, a cross-flow moving bed as the air reactor, and a combination of an inertial separator and a cyclone separator as the separation system. The actual thermal power inputs from the coal for the reported tests in this study were about 11 kW_{th} and the total duration reached about 70 h. The flow patterns and reaction characteristics of the whole system were investigated, and the effects of the fuel reactor temperature on the distributions of gas components in the two reactors were elucidated. At the fuel reactor temperature of 950 °C, the CO_2 yield, gas conversion, carbon capture efficiency, and total solid fuel conversion reached high values at 90.47%, 92.77%, 97.12%, and 98%, respectively. During the reported tests, the iron ore exhibited adequate reactivity and oxygen transport capacity, good cyclic stability, low tendency for agglomeration and high resistance to attrition.

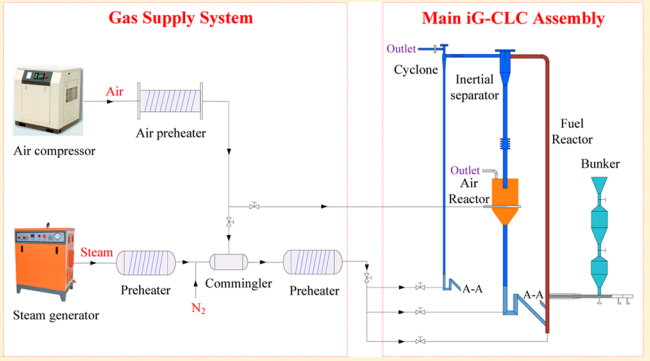

1. INTRODUCTION

Chemical looping combustion (CLC), which possesses an inherent feature of separating CO_2 during the combustion process, has been regarded as one of the most promising novel combustion technologies with low cost of CO_2 separation.[1,2] Since the introduction of CLC in 1980s, studies on CLC with gaseous fuels have been extensively developed from small-scale thermogravimetric analyzers (TGA) and fixed/fluidized beds[3−12] to pilot-scale units.[13−21] In recent years, in view of the advantages of solid fuels with respect to cost and reserves, the development of the solid fuel CLC is gaining momentum all over the world.[22−26]

A promising approach for the implementation of solid fuel CLC is called in situ gasification chemical looping combustion (iG-CLC).[27−29] In the iG-CLC process, the solid fuel is directly fed into the fuel reactor (FR) where it is mixed with the oxygen carrier (OC). Steam or CO_2 or their mixture is supplied into the FR as both the fluidizing gas and gasification agent. Thus, in the FR, the solid fuel is gasified by the gasification agent, and then the gasification products (e.g., CO, CH_4, H_2) are oxidized by the OC to CO_2 and H_2O. The OC reduced in the FR is then transferred into the air reactor (AR) where the OC is reoxidized by the air. Because the solid fuel and air are placed in two different reactors, the flue gas leaving the FR will only contain CO_2 and H_2O but not N_2. Thus, almost pure CO_2 can be obtained after the condensation of H_2O.

A suitable OC is very important for the successful operation of a CLC system. For the gaseous fuel CLC, some loss of the OC, primarily due to the attrition during the circulation process, is usually acceptable. Hence many synthetic OCs with high reactivity but also with high price can be good choices of OCs for future commercial CLC applications with gaseous fuels. However, compared with the gaseous fuel CLC, the iG-CLC technology has to face a serious issue of a much larger loss of the OC due to the mixing of the solid fuel and OC during the operation process, because the regular drain of fuel ash from the system will inevitably take away some OC particles.[30] In addition, the presence of organic sulfur in the solid fuel may lead to the deactivation of the OC.[31−33] In this context, the high-cost synthetic OCs may not be suitable for the large-scale iG-CLC applications. Therefore, some natural minerals (e.g.,

Received: August 8, 2016
Revised: September 19, 2016
Accepted: October 20, 2016
Published: October 20, 2016

DOI: 10.1021/acs.iecr.6b03028
Ind. Eng. Chem. Res. 2016, 55, 11775−11784

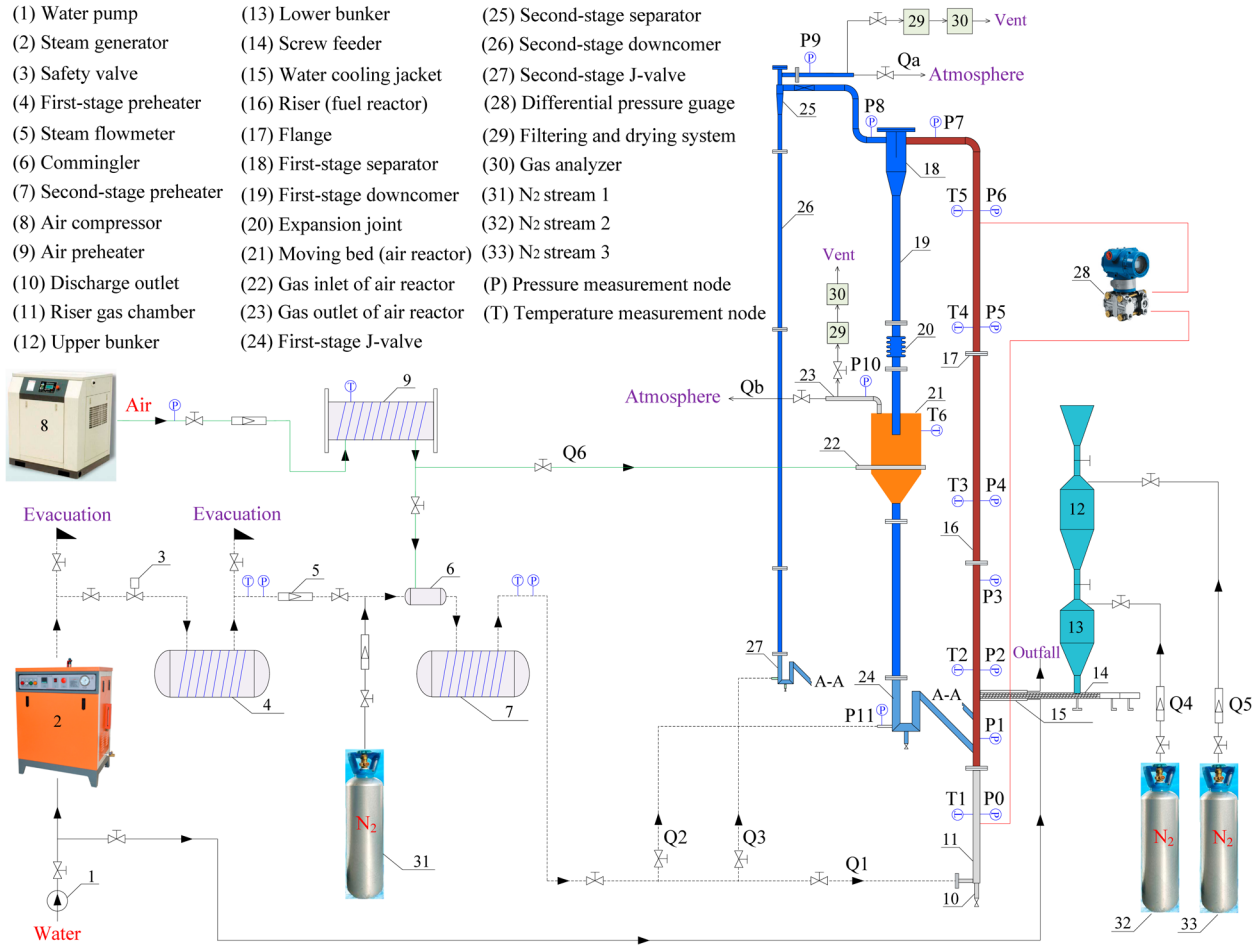

Figure 1. Schematic diagram of the 20 kW_{th} iG-CLC hot experimental setup.

iron ores,[24,26,34−36] manganese ores,[37] and copper ores[38]), by virtue of the low price but the relatively high reactivity, are attracting a lot of attention from iG-CLC researchers.

Currently, the studies of iG-CLC in the world have also entered into the early stage of pilot scale testing.[39] Berguerand and Lyngfelt[23,34,35] from Chalmers University of Technology took the lead in designing and operating a 10 kW_{th} pilot-scale unit with a bubbling fluidized bed (BFB) as the FR and a circulating fluidized bed (CFB) as the AR. Subsequently, some other units with different design concepts have also been successfully constructed and operated. Shen et al. from Southeast University developed two units of 1 kW_{th}[40] and 10 kW_{th}[25] which had a similar configuration with a spout fluidized bed as the FR and a CFB as the AR. Xiao et al.,[41] also from Southeast University, established a 50 kW_{th} pressurized iG-CLC unit of coal using an iron ore as the OC. The FR and AR of this unit were designed as a CFB and a BFB, respectively. Thon et al.[42] from Hamburg University of Technology constructed a 25 kW_{th} unit with a two-stage BFB as the FR and a CFB as the AR. The two-stage FR was specially designed for the purpose of enhancing the conversion of combustible gases. Markström et al.[43] from Chalmers University of Technology developed a 100 kW_{th} dual circulating fluidized bed (DCFB) unit with ilmenite as the OC. This kind of DCFB design can also be found in the units by Adánez et al.[44] from CSIC (20 kW_{th}), Ma et al.[45] from Huazhong University of Science and Technology (5 kW_{th}), and Ströhle et al.[46] from Technische Universität Darmstadt (1 MW_{th}) which is the world's biggest pilot-scale iG-CLC plant by far. Bayham et al.[47−49] from Ohio State University also developed a 25 kW_{th} coal-fired iG-CLC unit including a moving bed as the FR and a CFB as the AR.

In our previous studies, we proposed a novel iG-CLC system and successfully built and operated a cold experimental apparatus, preliminarily verifying the feasibility of this iG-CLC system.[32,33] The type of the FR was innovatively designed as a high-flux circulating fluidized bed (HFCFB) riser which can provide favorable gas−solid contact over the whole reactor height, just like what typical CFB FRs[43−45] can do. The high-flux operation can also greatly increase the solids flow rate and solids holdups (i.e., the OC inventory) in the FR, which will be very beneficial to the reaction efficiency of the OC. Moreover, the high OC inventory in the HFCFB FR can make up for the possible low OC reactivity, and hence provides the feasibility of using low-grade natural iron ores with lower reactivity as the OCs. The type of the AR was uniquely designed as a cross-flow moving bed in view of its advantages of low pressure drop, steady solids flow, and compact structure. In addition, a two-stage separation system including a low-efficiency inertial separator and a high-efficiency cyclone was specially designed for the purpose of the efficient gas−solid and solid−solid separations. During the iG-CLC process, the coal particles enter the bottom of the FR and react with the steam stream for gasification. The gasification products (e.g., CO and H_2) are subsequently oxidized by the OC particles to CO_2 and H_2O. The flue gas of the FR entrains the particles of the reduced OC

DOI: 10.1021/acs.iecr.6b03028
Ind. Eng. Chem. Res. 2016, 55, 11775−11784

and a fraction of unreacted char into the two-stage separation system. The first-stage inertial separator separates most of the large particles (mainly the OC particles) into the AR, but lets the flue gas and the fine particles (mainly the unreacted char particles) pass to the second-stage separator. The second-stage cyclone separator separates the fine char particles and sends them back to the FR for further reactions, but discharges the flue gas of the FR out of the system. The particles of the OC separated by the inertial separator further enter the AR for reoxidization, and then are sent back to the FR for circulation.

In this study, a pilot-scale 20 kW_{th} iG-CLC unit built on the concept proven with the cold experimental apparatus[32,33] was fully tested with a Chinese bituminous coal as the fuel and a natural iron ore from China as the OC. The operation stability, flow patterns and reaction characteristics of the whole system were investigated. The effects of the FR temperature on the distributions of gas components in the two reactors, carbon capture efficiency, and solid fuel conversion were established. According to the operation and reaction performance, the potential of the iron ore as the OC was also evaluated in terms of the reactivity, oxygen transport capacity, cyclic stability, tendency for agglomeration, and resistance to attrition and fragmentation.

2. EXPERIMENTAL SECTION

2.1. Materials. The OC used in this study was a calcined iron ore from China, which contains Fe_2O_3 (35.21%) and $CaSO_4$ (10.00%) as the reactive components, and SiO_2 (38.26%) and Al_2O_3 (8.22%) as the main inert components. It has an apparent density of 2558 kg/m^3 and a bulk density of 1535 kg/m^3 with a mean diameter of 0.55 mm. More details on this OC material and its redox properties can be found in our previous study.[50]

The fuel used was a Shenhua bituminous coal from the Inner Mongolia Autonomous Region of China.[33] The proximate and ultimate analyses of the coal are presented in Table S1. The mean diameter of the coal particles used in the experiments was 0.15 mm with the apparent density of 1270 kg/m^3.

2.2. Pilot-Scale Experimental Setup. Figure 1 schematically shows the pilot-scale hot experimental setup of the iG-CLC system. It comprises the main iG-CLC assembly, a gas supply system, a heating system, a data acquisition system, and other auxiliary parts.

2.2.1. Main iG-CLC Assembly. The main iG-CLC assembly is primarily composed of a FR (16), an AR (21), a two-stage separation system (18,25), two downcomers (19,26), two J-valves (24,27), an expansion joint (20), and a feeding system (12−15).

The FR (16) is an HFCFB riser with a height of 7 m and an inner diameter of 80 mm. The AR (21) is a cross-flow moving bed, mainly consisting of a gas inlet (22), a gas outlet (23), a cylindrical channel (0.53 m I.D. × 0.6 m height) and a cone channel (0.36 m height). The two-stage separation system contains a first-stage inertial separator (18) and a second-stage cyclone separator (25). The expansion joint (20) is installed between the first-stage inertial separator (18) and the AR (21) to absorb the thermal deformation of steel under the high temperatures. The feeding system includes an upper bunker (12), a lower bunker (13), a screw feeder (14), and a water cooling jacket (15).

2.2.2. Gas Supply System. The air stream from an air compressor (8) was introduced into the FR to circulate the OC particles at the start-up and shut-down stages. During the reaction stage, it was switched to the AR (21) to oxidize the OC particles.

The steam stream provided by a steam generator (2) was fed into the FR (16) during the reaction stage, which played the roles of not only the gasification agent but also the main fluidizing gas to circulate the OC particles.

A nitrogen (N_2) stream from the cylinder of liquid nitrogen (31) was fed into the FR (16) as the auxiliary fluidizing gas and the calibration gas. Another N_2 stream from the nitrogen cylinder (32) was introduced into the lower bunker (13) during the operating process to maintain a positive pressure differential between the feeding system and FR to ensure the successful feeding of coal into the FR. The third N_2 stream from the nitrogen cylinder (33) was fed into the upper bunker (12) to ensure the coal enters the lower bunker (13) smoothly during the reaction stage.

2.2.3. Heating System. The heating system comprises a preheating system and a reactor heating system. The preheating system includes a first-stage preheater (4), a second-stage preheater (7), and an air preheater (9). The steam and air streams were preheated to the designed temperatures before entering the reactors.

The FR including the riser gas chamber (11) is enclosed within four electric ovens and the AR is enclosed within an electric oven. These electric ovens were used to supply heat to the reactors at the stage of start-up and compensate the heat loss of the reactors during the reaction stage due to the imperfection of the external thermal insulation system.

2.2.4. Data Acquisition System. There are seven pressure monitoring nodes along the height of the FR (P0−P6), two nodes before and after the first-stage inertial separator (P7 and P8), one node at the outlet of the second-stage cyclone separator (P9), one node at the outlet of the AR (P10) and one node at the inlet of the first-stage J-valve (P11). The pressures of these monitoring nodes were measured by manometers and adjusted by the back pressure regulators. The pressure drop of the FR was measured by a differential pressure transducer (28) and the related data were logged on a computer continuously.

There are four temperature monitoring nodes for the real-time temperature of the FR (T2-T5), one node for the riser gas chamber (T1), one node for the AR (T6) and some other nodes for the first-stage preheater, the second-stage preheater, the air preheater, and so on. The temperatures of these monitoring nodes were measured by the thermocouples and the related data were continuously logged on a computer.

The flow rates of the air and nitrogen streams were controlled and measured by calibrated rotameters. The flow rate of the steam stream was measured by a steam flowmeter (5). The compositions of the flue gases from the two reactors were measured by a Germany MRU gas analyzer (30).

2.3. Experimental Procedure. Prior to the experiment, about 220 kg of the iron ore particles were added to the unit. At the beginning of the experiment, the electric ovens were started to heat the two reactors to a set temperature of 500 °C. After that, the N_2 stream (32) was introduced into the lower bunker to maintain the positive pressure differential of the feeding system to the FR. Then the preheating system was also started, and the air stream was introduced into the FR to drive the particles for circulation. When the particle circulation became stable, the electric ovens were started again to a target temperature (850−950 °C). After the target temperature was reached, the steam and the N_2 stream (31) were introduced to the FR. After that, the air stream was switched into the AR and

DOI: 10.1021/acs.iecr.6b03028
Ind. Eng. Chem. Res. 2016, 55, 11775−11784

matched into the original circulation system. When the whole system reached an ideal balance with the desired operation conditions, the coal particles were introduced into the FR continuously. At the same time, a small fraction of the flue gases at the outlets of the FR and AR were successively led to the filtering and drying system (29) and the gas analyzer (30) for gas analysis. During the shut-down stage, the air stream was switched back to the FR as the fluidization agent until the two reactors were cooled down.

2.4. Data Evaluation. *2.4.1. Solids Flux.* The solids flux (G_s) can be estimated from the gas velocity and the pressure drop of the CFB riser (i.e., FR).[23,33,40,51]

$$G_s = \frac{1}{g}\frac{\Delta P_{FR}}{\Delta h}(\overline{u}_{FR} - u_t) \tag{1}$$

where ΔP_{FR}, Δh and $\overline{u}_{FR}$ are the pressure drop, height, and mean gas velocity of the FR, respectively. u_t is the terminal velocity of particle, g is the acceleration of gravity.

Previous studies found that the solids flux calculated by eq 1 could be significantly overestimated.[33,40,51] In this study, the corrected solids flux ($G_{s,c}$) was given on the basis of the batch experiments in the 20 kW_{th} unit and the previous cold experiments:

$$G_{s,c} = 0.25G_s \tag{2}$$

2.4.2. Apparent Solids Holdup. The cross-sectional apparent solids holdup (ε_s) in the FR can be estimated from the local pressure drop.[32,33,52−55]

$$\Delta P_Z/\Delta Z \approx [\rho_s\varepsilon_s + \rho_g(1 - \varepsilon_s)]g \tag{3}$$

where ΔP_z is the local pressure drop at two adjacent elevations of the FR.

2.4.3. CO_2 Yield. The CO_2 yield ($f_{CO_2,FR}$) represents the CO_2 fraction in the total gaseous carbon leaving the FR.[23,45]

$$f_{CO_2,FR} = \frac{X_{CO_2,FR}}{X_{CO_2,FR} + X_{CO,FR} + X_{CH_4,FR}} \tag{4}$$

where $X_{CO_2,FR}$, $X_{CO,FR}$ and $X_{CH_4,FR}$ are the measured molar fractions of CO_2, CO, and CH_4 in the dry flue gas of the FR, respectively.

2.4.4. Oxygen Demand and Gas Conversion. The oxygen demand (Ω_{OD}) represents the fraction of oxygen lacking to achieve a complete combustion of the carbon-containing gases leaving the FR.[23,45]

$$\Omega_{OD} = \frac{0.5X_{CO,FR} + 2X_{CH_4,FR}}{\Phi_0(X_{CO_2,FR} + X_{CO,FR} + X_{CH_4,FR})} \tag{5}$$

where Φ_0 is the oxygen/carbon ratio, that is, the ratio of moles of oxygen needed to convert the fuel completely per mole of carbon in the fuel.

The gas conversion (η_g) represents the conversion of the carbon-containing gases leaving the FR.[43,45]

$$\eta_g = 1 - \Omega_{OD} \tag{6}$$

2.4.5. Carbon Capture Efficiency. The carbon capture efficiency (η_{CC}) is the ratio of carbon-containing gas flow leaving the FR to the total carbon-containing gas flow leaving the system.[23,41,45]

$$\eta_{CC} = \frac{F_{C,FR}}{F_{C,FR} + F_{C,AR}} \tag{7}$$

where $F_{C,FR}$ and $F_{C,AR}$ are the carbonaceous gas flow leaving the FR and the AR, respectively.

$F_{C,FR}$ can be obtained on the basis of the known flow of nitrogen added into the FR ($F_{N_2,FR}$):[23,40]

$$F_{C,FR} = \frac{X_{CO_2,FR} + X_{CO,FR} + X_{CH_4,FR}}{X_{N_2,FR}} \times F_{N_2,FR} \tag{8}$$

where $X_{N_2,FR}$ is the molar fraction of N_2 in the dry flue gas of the FR.

$F_{C,AR}$ can be calculated using the known air flow entering the AR ($F_{air,AR}$):[23,45]

$$F_{C,AR} = \frac{X_{CO_2,AR} + X_{CO,AR} + X_{CH_4,AR}}{X_{N_2,AR}} \times (F_{air,AR} \times 0.79) \tag{9}$$

where $X_{CO_2,AR}$, $X_{CO,AR}$, $X_{CH_4,AR}$ and $X_{N_2,AR}$ are the molar fractions of CO_2, CO, CH_4 and N_2 in the flue gas of the AR, respectively.

2.4.6. Solid Fuel Conversion. According to the mass balance of carbon, the carbon added with the solid fuel ($F_{C,Fuel}$) equals to the sum of the total gaseous carbon leaving the system and the carbon leaving the process in the form of unconverted char.[23]

The single-pass solid fuel conversion η_{Fuel} represents the proportion of the carbon added with the solid fuel ($F_{C,Fuel}$) converted into the gaseous carbon in a single pass of the FR ($F_{C,FR} + F_{C,AR}$).

$$\eta_{Fuel} = \frac{F_{C,FR} + F_{C,AR}}{F_{C,Fuel}} \tag{10}$$

The single-pass solid fuel conversion η_{Fuel} is an important factor affecting the practical output of thermal power. In this work, in order to obtain more accurate values of η_{Fuel}, the transmission of the unreacted char separated by the second-stage cyclone separator to the FR was suspended during the measurement stage. Thus, it can be ensured that the solid fuel added into the FR during the reaction process just came from the coal feeder (i.e., $F_{C,Fuel}$).

Certainly, the total conversion of solid fuel $\eta_{Fuel,t}$ should be higher than the single-pass solid fuel conversion η_{Fuel} because $\eta_{Fuel,t}$ also includes the conversion of the recirculated char from the separation system on the basis of η_{Fuel}. As shown in eq 11, the total conversion of solid fuel $\eta_{Fuel,t}$ can be estimated according to the carbon flow of fly ash leaving the separation system.[25]

$$\eta_{Fuel,t} = 1 - \frac{F_{C,fly\ ash}}{F_{C,Fuel}} \tag{11}$$

where $F_{C,fly\ ash}$ is the carbon flow of fly ash leaving the separation system. Here, it should be noted that the value of $F_{C,fly\ ash}$ is directly determined by the performance of the two-stage separation system. Specifically, the higher the recirculation efficiency of the unreacted char due to the two-stage separation performance is, the lower the carbon flow of fly ash leaving the separation system (i.e., $F_{C,fly\ ash}$) will be, and thus the higher the total conversion of solid fuel (i.e., $\eta_{Fuel,t}$) will be.

DOI: 10.1021/acs.iecr.6b03028
Ind. Eng. Chem. Res. 2016, 55, 11775−11784

3. RESULTS AND DISCUSSION

As shown in Table 1, a series of tests were carried out with the FR temperature ranging from 870 to 950 °C while the temperature of the AR was kept constant at 950 °C. The thermal input power corresponding to the used coal feed rate was about 11 kW with a constant excess air coefficient of 1.1. The solids flux was maintained at around 250 kg/(m^2 s). The steam supply, which was used as the main gasifying/fluidizing gas in the FR, was kept around two times of the minimum gas flow rate needed for the particle circulation. The nitrogen streams with a total flow rate of 6 N m^3/h were introduced into the bottom of the FR to determinate the flow rate of exhaust gas from the FR. The total duration of the tests reached about 70 h including 20 h under stable reaction states.

Table 1. Main Operating Conditions and Parameters for the iG-CLC Tests

test	FR temp (°C)	AR temp (°C)	coal feed rate (kg/h)	solids flux (kg/(m^2 s))	stable reaction time (h)
1	950	950	1.5	~250	~3
2	950	950	1.5	~250	~2
3	950	950	1.5	~250	~2.5
4	900	950	1.5	~250	~3.5
5	900	950	1.5	~250	~2
6	870	950	1.5	~250	~4
7	870	950	1.5	~250	~3

Among all tests, test 1 is defined as the reference test to present the primary flow behaviors and reaction characteristics of the proposed iG-CLC system. Tests 1, 4, and 6 are selected to study the effect of the FR temperature on the reaction performance of the whole system. Tests 2 and 3 are the repetition tests of test 1. Similarly, test 5 and test 7 are the repetition tests of test 4 and test 6, respectively.

3.1. Heating and Flow Characteristics. In hot iG-CLC experiments, the visualization is usually impossible due to the high operation temperatures and/or pressures, and hence the operation stability of the system can only be judged by monitoring the fluctuations of temperatures and pressures in real time. Because the flow and reaction characteristics in the FR directly affect the performance of the whole iG-CLC system, the monitoring of the state of the FR is particularly important.

Figure 2 illustrates the real-time curves of the temperature and differential pressure ($P0$–$P6$) in the FR during the heating and reaction stages. With the automatic control of temperature, the FR temperature went up steadily in the heating stage and maintained with slight oscillations around the target value in the reaction stage as a whole. It should be noted that the temperature fluctuations occurring in the heating stage around 500 °C were caused by the introduction of air stream for particle circulation. On the other hand, obvious fluctuations with time were observed from the curve of differential pressure. This indicates the achievement of intense turbulence in the FR during the operating process, which was beneficial to the gas–solid contacts and reactions. Moreover, the fluctuations of the differential pressure remained constant during the whole process, indicating the smooth control of the gas flow and steady circulation of particles.

Figure 3 shows the whole-system pressure profiles of the iG-CLC unit under the reference test conditions. The pressure fields between different parts were smoothly connected,

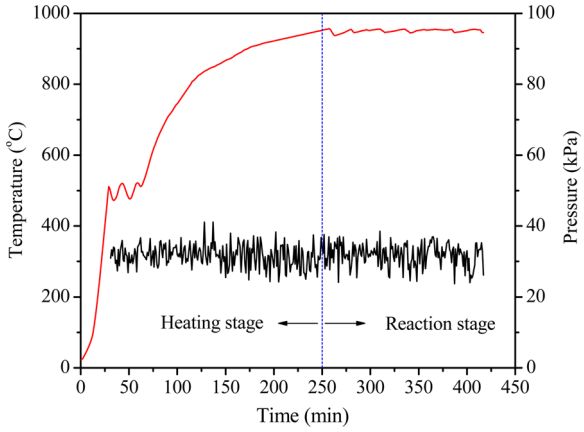

Figure 2. Real-time curves of the temperature and differential pressure in the FR with the reference test.

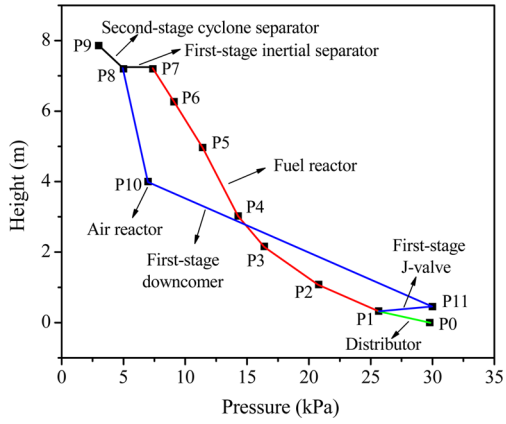

Figure 3. Whole-system pressure profiles of the iG-CLC unit under the reference test conditions.

indicating a good match of components and the stability of the system. We also observed an obvious decay of pressure (about 18.3 kPa) along the FR height. Moreover, the pressure drop of the separation system reached about 4.4 kPa. The above observations are consistent with the results of our previous cold experiments.[32,33]

Figure 4 presents the axial profile of the apparent solids holdup along the FR height. The solids holdup rapidly decreased along the axial direction at the bottom region, and

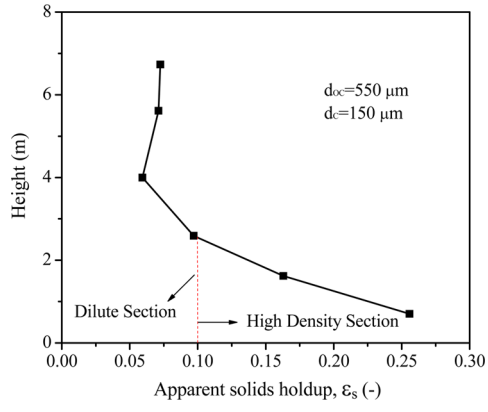

Figure 4. Axial profile of apparent solids holdup along the FR height with the reference test.

DOI: 10.1021/acs.iecr.6b03028
Ind. Eng. Chem. Res. 2016, 55, 11775–11784

then leveled off in the upper region. Generally, the solids holdup exhibited an approximately exponential distribution along the height of the FR. It could be further observed that over one-third of the FR height achieved the high-density structure ($\varepsilon_s \geq 0.1$), and the solids holdups in the dilute section were all higher than 0.05. This verifies the positive effect of high-flux operation on the solids holdups and further the gas–solid contact efficiency in the FR.[32,33]

During the 70 h operation under the high-temperature and high-flux conditions, the iron ore used in this study exhibited a low tendency for agglomeration and defluidization, and a high resistance to attrition and fragmentation. Meanwhile, the iron ore OC experienced hundreds of redox cycles during the total reaction time (20 h), revealing its favorable cyclic stability.

3.2. Reaction Characteristics. Figure 5 shows the concentration variations of gas compositions at the outlet of the FR with time under the reference test conditions. The time-averaged concentrations of CO_2, CO, and CH_4 were 17.43%, 1.39%, and 0.47%, respectively. The fluctuations in gas concentrations were largely due to the fluctuations of the coal feed rate. Such imperfection in the control of fuel feed rate also occurred in some other researchers' units.[23,45]

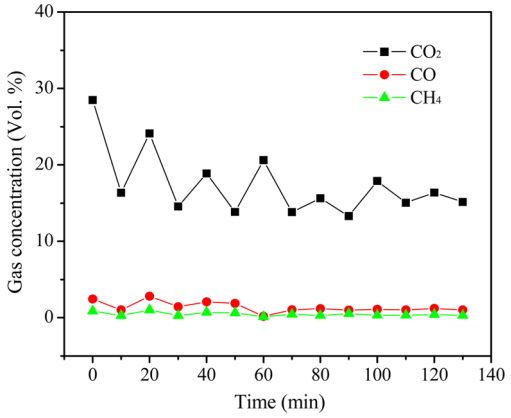

Figure 5. Concentration variations of gas compositions at the outlet of the FR with time (reference test).

Figure 6 presents the variations of CO_2 yield and oxygen demand at the outlet of the FR with time under the reference test. It could be observed that the CO_2 yield under the reference test reached a stable average value of 90.47% and the other 9.53% as CO and CH_4. Correspondingly, the oxygen demand stabilized at a low value of 7.23%. Thus, according to eq 6, the gas conversion could be calculated to be 92.77%. The high values of CO_2 yield and gas conversion indicated the favorable reaction performance of the HFCFB FR because of the sufficient solids holdups, and adequate reactivity and oxygen transport capacity of the iron ore OC. Meanwhile, the smooth trends of CO_2 yield and oxygen demand with time illustrated the good cyclic stability of the iron ore OC during the operation.

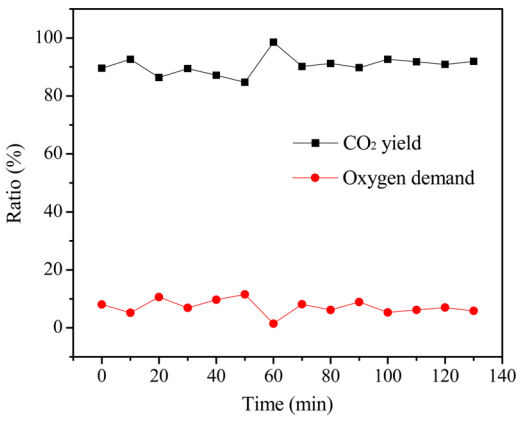

Figure 6. Variations of CO_2 yield and oxygen demand at the outlet of the FR with time for the reference test.

In the AR, the oxygen was consumed for oxidizing the OC under a reduced state together with a small fraction of unreacted char from the FR. Figure 7 shows the concentration fluctuations of O_2 and CO_2 with time at the outlet of the AR. Only slight fluctuations with time were observed for both O_2 and CO_2. Compared with the O_2 concentration in the air (i.e., 21%), the measured average concentration of O_2 at the outlet of the AR was only 8.66%, indicating a successful transfer of oxygen from the air to the reduced OC. Meanwhile, the average concentration of CO_2 was only about 0.63%, revealing only a small fraction of oxygen was consumed to burn the char. This further verifies the high selective separation efficiency of the first-stage inertial separator. Specifically, the inertial separator successfully separated most of the large OC particles to the AR for regeneration, but let most of the fine char particles head for the second-stage cyclone separator for recirculation and further reactions.[33]

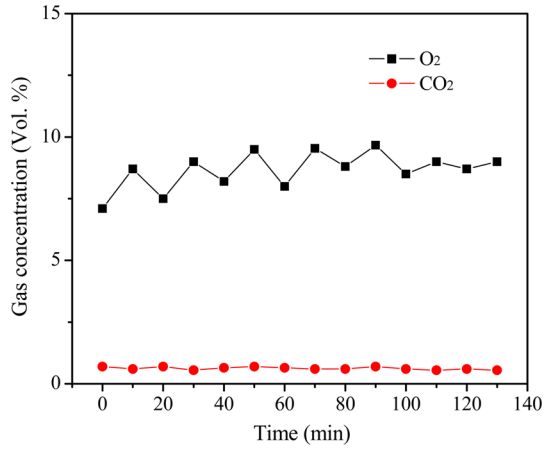

Figure 7. Concentration fluctuations of O_2 and CO_2 with time at the outlet of the AR for the reference test.

Moreover, by comparing the temporal distributions of CO_2 at the outlet of the FR (see Figure 5) and O_2 at the outlet of the AR (see Figure 7), we observed a close relationship between the two parameters. Whenever the CO_2 concentration at the outlet of the FR reached a peak, the O_2 at the outlet of the AR would fall into a valley accordingly. This is mainly because more coal was introduced into the FR at such moments, and thus more CO_2 was produced and more OC was reduced so that more oxygen in the AR was consumed.

Figure 8 presents the time averages of carbon capture efficiency η_{CC} and single-pass solid fuel conversion η_{Fuel} relating to the reference test. The carbon capture efficiency reached 97.12%, indicating most of the carbonaceous gas flow left the system via the FR. This is mainly attributed to the high selective separation efficiency of the first-stage inertial separator, which is consistent with the previous analysis of the CO_2 concentration

DOI: 10.1021/acs.iecr.6b03028
Ind. Eng. Chem. Res. 2016, 55, 11775–11784

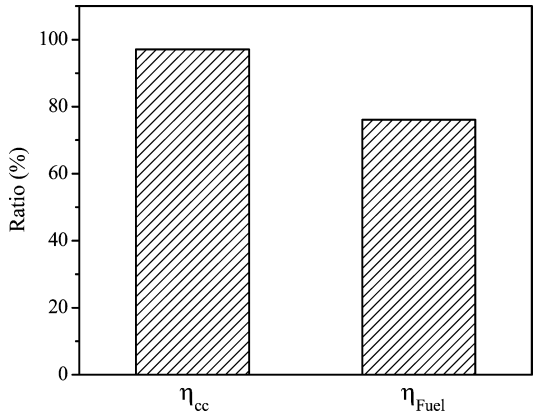

Figure 8. Carbon capture efficiency and single-pass solid fuel conversion with the reference test.

at the outlet of the AR. On the other hand, the single-pass solid fuel conversion reached 76.09%, meaning that over $^3/_4$ of the carbon added with the fuel had been converted into the gaseous carbon just through a single pass in the FR. In addition, based on the measured value of the carbon flow of fly ash leaving the separation system, the total solid fuel conversion $\eta_{Fuel,t}$ could be estimated to be around 98% (see eq 11), indicating the achievement of the high-efficiency recirculation of the unreacted char with the help of the specific two-stage separation system.

3.3. Effect of the FR Temperature. Temperature in the FR is one of the main operating variables affecting the CO_2 capture efficiency and fuel conversion of an iG-CLC system.[31,35,40,56,57] Tests 1, 4, and 6 were performed with different temperatures ranging from 870 to 950 °C to investigate the effect of the FR temperature on the reaction performance of the whole system when the other operating parameters were kept more or less constant.

Figure 9 shows the variation of CO_2 yield with different FR temperatures. We observed a positive effect of the FR

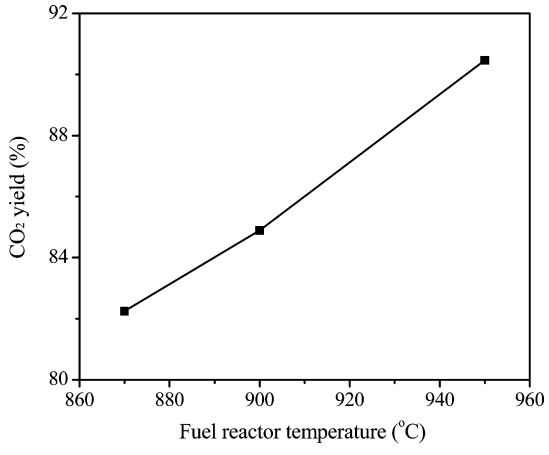

Figure 9. Effect of the FR temperature on the CO_2 yield.

temperature on the CO_2 yield at the FR outlet. The CO_2 yield was about 82.25% at 870 °C and increased to 90.47% at 950 °C. The increase in the CO_2 yield with a higher FR temperature is mainly attributed to the increase in the OC reactivity, which could promote the conversion of gaseous carbon to CO_2.

Figure 10 presents the effect of the FR temperature on the gas compositions at the outlet of the AR. When the FR

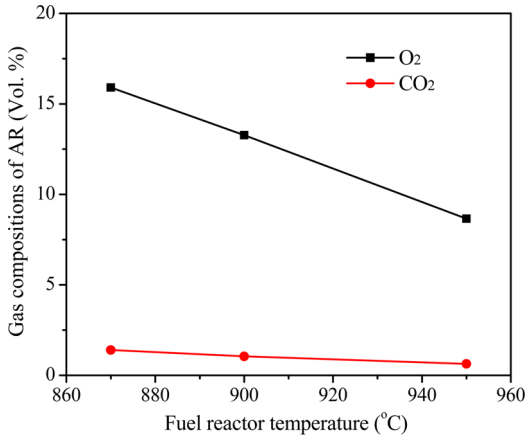

Figure 10. Effect of the FR temperature on the gas compositions at the outlet of the AR.

temperature increased from 870 to 950 °C, the concentrations of O_2 and CO_2 decreased from 15.91% to 8.66% and 1.4% to 0.63%, respectively. The increase of the FR temperature accelerated the gasification rate, and thus more char was consumed and more gasification products were generated. The increase of the gasification products resulted in more reduction of the OC in the FR, and further more consumption of oxygen in the AR to reoxidize the OC, which was the reason why the O_2 concentration in the flue gas of the AR decreased with the increase of the FR temperature. Moreover, the increase of the char consumption in the FR directly resulted in the decrease of the residual char at the outlet of the FR, and hence the decrease of char entering the AR, which could explain why the increase of the FR temperature led to the decrease of the CO_2 concentration in the flue gas of the AR.[40]

Figure 11 shows the variations of the carbon capture efficiency η_{CC} and single-pass solid fuel conversion η_{Fuel} as a

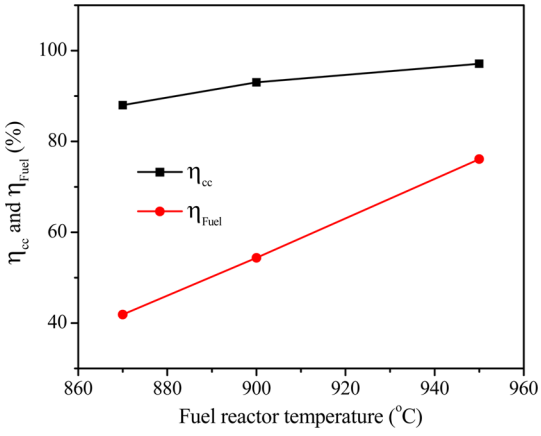

Figure 11. Variations of the carbon capture efficiency η_{CC} and single-pass solid fuel conversion η_{Fuel} as a function of the FR temperature.

function of the FR temperature. The time average of the carbon capture efficiency was 93.02% for the FR temperature of 870 °C and increased to 97.12% when the temperature was increased to 950 °C. According to the previous analysis, the increase of the FR temperature promoted the gasification rate

DOI: 10.1021/acs.iecr.6b03028
Ind. Eng. Chem. Res. 2016, 55, 11775−11784

of char, which further led to the increase of the carbonaceous gas flow in the FR and the decrease of the carbonaceous gas flow in the AR. Hence, according to eq 7, the carbon capture efficiency would have a corresponding increase. On the other hand, the increase of the FR temperature from 870 to 950 °C also promoted the single-pass solid fuel conversion from 41.88% to 76.09%, which was believed to be related to the higher gasification rate of char and hence the increase of the carbonaceous gas flow leaving the system (see eq 10).

3.4. Data Uncertainty Analysis. A series of repetition tests were conducted in order to reveal the data confidence level. As mentioned earlier, tests 2 and 3 are the repetition tests of test 1 while test 5 and test 7 are the repetition tests of test 4 and test 6, respectively. In this section, CO_2 yield was selected as a representative of performance indicators for the data uncertainty analysis.

Figure 12 shows the fluctuations of CO_2 yield among repetition tests as a function of the FR temperature. It could be found that, at a given FR temperature, the average CO_2 yields among repetition tests were close to each other, and the maximum relative error was less than 5%. This indicates that the data acquired from the experiments should be credible and reproducible. In addition, the OC circulation flux, which is directly related to the CO_2 yield, was steady and controllable during the operation process.

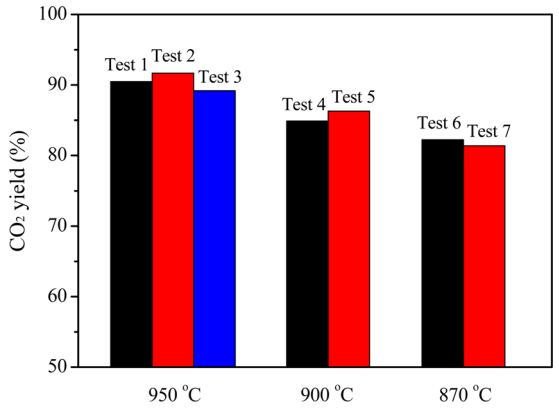

Figure 12. Fluctuations of CO_2 yield among repetition tests as a function of the FR temperature.

3.5. Performance Comparison with Other iG-CLC Units. To better evaluate the potential of our iG-CLC system, we carried out a comparison of its reaction performance with those of other iG-CLC units. As shown in Table 2, the main operating conditions (e.g., gasification agent type, thermal input power, solids inventory in the FR, and FR temperature) used in our reference test were very similar to those in previous experiments by Shen et al.[25] and Berguerand and Lyngfelt,[23] except that the FR types in their units were typical bubbling/spout fluidized beds while in this study it is an HFCFB riser.

It could be found that the novel iG-CLC unit evaluated by this study, although using a low-grade iron ore as the OC, showed adequate CO_2 yield (90.47%), comparable to those of the previous iG-CLC units.[23,25] This is mainly because that, in comparison with the typical bubbling/spout fluidized beds, the HFCFB riser as the FR provided favorable gas−solid contacts over the whole reactor height. Moreover, the realization of the high-flux operation greatly increased the solids holdups and further enhanced the gas−solid contact and reaction efficiencies in the FR, thus overcoming the shortcoming of a typical CFB FR in terms of low FR solids inventory.

Table 2. Comparison of Reaction Performance among Different iG-CLC Units

description	Shen et al.[25]	Berguerand and Lyngfelt[23]	this work
FR type	spout-fluid bed	lower BFB and upper CFB	HFCFB
AR type	CFB	CFB	moving bed
material of the OC	NiO/$NiAl_2O_4$	ilmenite	iron ore
gasification agent type	H_2O/CO_2	H_2O	H_2O
thermal input (kW_{th})	8.3	3.3	11
FR solids inventory (kg/MW_{th})	∼1300	∼1700	∼1100
FR temperature (°C)	970	950	950
CO_2 yield (%)	95.2	78−81	90.47
carbon capture efficiency (%)	∼84.2	82−96	97.12
solid fuel conversion (%)	>92.8	50−80	∼98

In addition, the high-efficiency recirculation of residual char in the FR was achieved in our system with the help of a specific two-stage separation system, thus ensuring high values of carbon capture efficiency (97.12%) and total conversion of solid fuel (about 98%). It should be noted that, because of the poor performance of the FR cyclone, much lower conversions of solid fuel (only 50−80%) were obtained in the experiments by Berguerand and Lyngfelt.[23] However, with a similar efficiency of full-scale cyclone, the solid fuel conversion in their unit could also increase to a high value (about 98−99%).

Overall, the novel iG-CLC apparatus developed by us exhibited high competitiveness against the previous units in terms of CO_2 yield, carbon capture efficiency, and solid fuel conversion, indicating its good potential for applications with future large-scale iG-CLC power plants.

4. CONCLUSIONS

On the basis of our design and operational experience achieved with the cold experimental apparatus of the novel iG-CLC system, we have built and successfully operated a 20 kW_{th} hot iG-CLC unit with a Chinese bituminous coal as the fuel and a natural iron ore as the oxygen carrier. After successful commissioning, this hot unit ran for a total duration of about 70 h including 20 h under stable reaction states. The following conclusions can be drawn from the present study:

(1) Both stability in operation and good reaction performance were achieved with the hot unit, verifying the operational feasibility and potential of the novel iG-CLC system.

(2) The HFCFB riser as the fuel reactor provided favorable gas−solid contacts over the whole reactor height together with adequate solids holdups, which could greatly promote the gas−solid reaction efficiency in the fuel reactor. The cross-flow moving bed as the air reactor achieved a steady transfer of oxygen from the air to the reduced oxygen carrier. The specific two-stage separation system implemented the efficient separation among the flue gas, unreacted char and oxygen carrier leaving the fuel reactor, thus ensuring a high carbon capture efficiency and an ideal total conversion of solid fuel.

DOI: 10.1021/acs.iecr.6b03028
Ind. Eng. Chem. Res. 2016, 55, 11775−11784

(3) An increase in the fuel reactor temperature brought positive effects on both the carbon capture efficiency and the solid fuel conversion.
(4) The low-cost iron ore exhibited adequate reactivity and oxygen transport capacity, good cyclic stability, low tendency for agglomeration, and high resistance to attrition and fragmentation during the 70-h operation under the high temperature and high-flux conditions, indicating its good potential for applications with future commercial iG-CLC power plants.

■ ASSOCIATED CONTENT

Supporting Information

The Supporting Information is available free of charge on the ACS Publications website at DOI: 10.1021/acs.iecr.6b03028.

Proximate and ultimate analyses (air-dried basis) of the Shenhua bituminous coal (Table S1)(PDF)

■ AUTHOR INFORMATION

Corresponding Authors

*Tel.: +86-25-83792506. Fax: +86-25-83792506. E-mail: bsjin@seu.edu.cn.
*Tel.: +44-115-8467674. Fax: +44-115-9513159. E-mail: liu.hao@nottingham.ac.uk.

Notes

The authors declare no competing financial interest.

■ ACKNOWLEDGMENTS

This work was supported by the National Natural Science Foundation of China (51276038, 51076029); the UK Engineering and Physical Sciences Research Council (EP/G063176/1, EP/I010912/1); the Ministry of Science and Technology of China (China-EU International Collaboration Project 2010DFA61960).

■ REFERENCES

(1) Fan, L. S. *Chemical Looping Systems for Fossil Energy Conversions*; Wiley-AIChE: New York, 2010.
(2) Lyngfelt, A.; Leckner, B.; Mattisson, T. A fluidized-bed combustion process with inherent CO_2 separation; application of chemical-looping combustion. *Chem. Eng. Sci.* **2001**, *56*, 3101.
(3) Ishida, M.; Jin, H.; Okamoto, T. A fundamental study of a new kind of medium material for chemical-looping combustion. *Energy Fuels* **1996**, *10*, 958.
(4) Jin, H.; Okamoto, T.; Ishida, M. Development of a novel chemical-looping combustion: synthesis of a solid looping material of $NiO/NiAl_2O_4$. *Ind. Eng. Chem. Res.* **1999**, *38*, 126.
(5) Mattisson, T.; Lyngfelt, A.; Cho, P. The use of iron oxide as an oxygen carrier in chemical-looping combustion of methane with inherent separation of CO_2. *Fuel* **2001**, *80*, 1953.
(6) Ishida, M.; Yamamoto, M.; Ohba, T. Experimental results of chemical-looping combustion with $NiO/NiAl_2O_4$ particle circulation at 1200 °C. *Energy Convers. Manage.* **2002**, *43*, 1469.
(7) Mattisson, T.; Järdnäs, A.; Lyngfelt, A. Reactivity of some metal oxides supported on alumina with alternating methane and oxygen application for chemical-looping combustion. *Energy Fuels* **2003**, *17*, 643.
(8) Cho, P.; Mattisson, T.; Lyngfelt, A. Comparison of iron-, nickel-, copper- and manganese-based oxygen carriers for chemical-looping combustion. *Fuel* **2004**, *83*, 1215.
(9) García-Labiano, F.; Adánez, J.; de Diego, L. F.; Gayán, P.; Abad, A. Effect of pressure on the behavior of copper-, iron-, and nickel-based oxygen carriers for chemical-looping combustion. *Energy Fuels* **2006**, *20*, 26.
(10) Abad, A.; Adánez, J.; García-Labiano, F.; de Diego, L. F.; Gayán, P.; Celaya, J. Mapping of the range of operational conditions for Cu-, Fe-, and Ni-based oxygen carriers in chemical-looping combustion. *Chem. Eng. Sci.* **2007**, *62*, 533.
(11) Cuadrat, A.; Abad, A.; Adánez, J.; de Diego, L. F.; García-Labiano, F.; Gayán, P. Behavior of ilmenite as oxygen carrier in chemical-looping combustion. *Fuel Process. Technol.* **2012**, *94*, 101.
(12) Gu, H.; Shen, L.; Xiao, J.; Zhang, S.; Song, T.; Chen, D. Evaluation of the effect of sulfur on iron-ore oxygen carrier in chemical-looping combustion. *Ind. Eng. Chem. Res.* **2013**, *52*, 1795.
(13) Ryu, H. J.; Jin, G. T.; Bae, D. H.; Yi, C. K. Continuous operation of a 50 kW_{th} chemical-looping combustor: long-term operation with Ni-and Co-based oxygen carrier particles. In 5th China-Korea Joint Workshop on Clean Energy Technology, October, 2004.
(14) Lyngfelt, A.; Thunman, H. Construction and 100 h of operational experience of a 10-kW chemical-looping combustor. *Carbon dioxide capture for storage in deep geologic formations-results from the CO_2 capture project*; Elsevier BV: Amsterdam, The Netherlands, 2005; Vol. *1*, p 625.
(15) Abad, A.; Mattisson, T.; Lyngfelt, A.; Rydén, M. Chemical-looping combustion in a 300W continuously operating reactor system using a manganese-based oxygen carrier. *Fuel* **2006**, *85*, 1174.
(16) de Diego, L. F.; García-Labiano, F.; Gayán, P.; Celaya, J.; Palacios, J. M.; Adánez, J. Operation of a 10 kW_{th} chemical-looping combustor during 200 h with a $CuO-Al_2O_3$ oxygen carrier. *Fuel* **2007**, *86*, 1036.
(17) Adánez, J.; Dueso, C.; de Diego, L. F.; García-Labiano, F.; Gayán, P.; Abad, A. Methane combustion in a 500 W_{th} chemical-looping combustion system using an impregnated Ni-based oxygen carrier. *Energy Fuels* **2008**, *23*, 130.
(18) Pröll, T.; Mayer, K.; Bolhàr-Nordenkampf, J.; Kolbitsch, P.; Mattisson, T.; Lyngfelt, A.; Hofbauer, H. Natural minerals as oxygen carriers for chemical looping combustion in a dual circulating fluidized bed system. *Energy Procedia* **2009**, *1*, 27.
(19) Forero, C. R.; Gayán, P.; de Diego, L. F.; Abad, A.; García-Labiano, F.; Adánez, J. Syngas combustion in a 500 W_{th} chemical-looping combustion system using an impregnated Cu-based oxygen carrier. *Fuel Process. Technol.* **2009**, *90*, 1471.
(20) Kolbitsch, P.; Bolhar-Nordenkampf, J.; Pröll, T.; Hofbauer, H. Comparison of two Ni-based oxygen carriers for chemical looping combustion of natural gas in 140 kW continuous looping operation. *Ind. Eng. Chem. Res.* **2009**, *48*, 5542.
(21) Ma, J.; Zhao, H.; Tian, X.; Wei, Y.; Zhang, Y.; Zheng, C. Continuous Operation of Interconnected Fluidized Bed Reactor for Chemical Looping Combustion of CH_4 Using Hematite as Oxygen Carrier. *Energy Fuels* **2015**, *29*, 3257.
(22) Cao, Y.; Pan, W. P. Investigation of Chemical looping combustion by solid fuels: 1 Process analysis. *Energy Fuels* **2006**, *20*, 1836.
(23) Berguerand, N.; Lyngfelt, A. Design and operation of a 10 kW_{th} chemical-looping combustor for solid fuels-testing with South African coal. *Fuel* **2008**, *87*, 2713.
(24) Leion, H.; Mattisson, T.; Lyngfelt, A. Solid Fuels in Chemical-Looping Combustion. *Int. J. Greenhouse Gas Control* **2008**, *2*, 180.
(25) Shen, L. H.; Wu, J. H.; Xiao, J. Experiments on chemical looping combustion of coal with a NiO based oxygen carrier. *Combust. Flame* **2009**, *156*, 721.
(26) Xiao, R.; Song, Q. L.; Song, M.; Lu, Z. J.; Zhang, S.; Shen, L. H. Pressurized chemical-looping combustion of coal with an iron ore-based oxygen carrier. *Combust. Flame* **2010**, *157*, 1140.
(27) Abad, A.; Gayán, P.; de Diego, L. F.; García-Labiano, F.; Adánez, J. Fuel reactor modelling in chemical-looping combustion of coal: 1. Model formulation. *Chem. Eng. Sci.* **2013**, *87*, 277.
(28) García-Labiano, F.; de Diego, L. F.; Gayán, P.; Abad, A.; Adánez, J. Fuel reactor modelling in chemical-looping combustion of coal: 2-simulation and optimization. *Chem. Eng. Sci.* **2013**, *87*, 173.
(29) Cuadrat, A.; Abad, A.; Gayán, P.; de Diego, L. F.; García-Labiano, F.; Adánez, J. Theoretical approach on the CLC performance with solid fuels: optimizing the solids inventory. *Fuel* **2012**, *97*, 536.

DOI: 10.1021/acs.iecr.6b03028
Ind. Eng. Chem. Res. 2016, 55, 11775−11784

(30) Adánez, J.; Cuadrat, A.; Abad, A.; Gayán, P.; de Diego, L. F.; García-Labiano, F. Ilmenite activation during consecutive redox cycles in chemical-looping combustion. *Energy Fuels* **2010**, *24*, 1402.
(31) Wang, X.; Jin, B.; Zhang, Y.; Zhang, Y.; Liu, X. Three Dimensional Modeling of a Coal-Fired Chemical Looping Combustion Process in the Circulating Fluidized Bed Fuel Reactor. *Energy Fuels* **2013**, *27*, 2173.
(32) Wang, X.; Jin, B.; Liu, X.; Zhang, Y.; Liu, H. Experimental investigation on flow behaviors in a novel in situ gasification chemical looping combustion apparatus. *Ind. Eng. Chem. Res.* **2013**, *52*, 14208.
(33) Wang, X.; Jin, B.; Liu, H.; Wang, W.; Liu, X.; Zhang, Y. Optimization of in-situ Gasification Chemical Looping Combustion through Experimental Investigations with a Cold Experimental System. *Ind. Eng. Chem. Res.* **2015**, *54*, 5749.
(34) Berguerand, N.; Lyngfelt, A. The use of petroleum coke as fuel in a 10 kW_{th} chemical-looping combustor. *Int. J. Greenhouse Gas Control* **2008**, *2*, 169.
(35) Berguerand, N.; Lyngfelt, A. Chemical-looping combustion of petroleum coke using ilmenite in a 10 kW_{th} unit-high-temperature operation. *Energy Fuels* **2009**, *23*, 5257.
(36) Berguerand, N.; Lyngfelt, A. Batch testing of solid fuels with ilmenite in a 10 kW_{th} chemical-looping combustor. *Fuel* **2010**, *89*, 1749.
(37) Arjmand, M.; Leion, H.; Lyngfelt, A.; Mattisson, T. Use of manganese ore in chemical-looping combustion (CLC)-Effect on steam gasification. *Int. J. Greenhouse Gas Control* **2012**, *8*, 56.
(38) Zhao, H.; Wang, K.; Fang, Y.; Ma, J.; Mei, D.; Zheng, C. Characterization of natural copper ore as oxygen carrier in chemical-looping with oxygen uncoupling of anthracite. *Int. J. Greenhouse Gas Control* **2014**, *22*, 154.
(39) Lyngfelt, A. Chemical-looping combustion of solid fuels-status of development. *Appl. Energy* **2014**, *113*, 1869.
(40) Shen, L.; Wu, J.; Gao, Z.; Xiao, J. Characterization of chemical looping combustion of coal in a 1 kW_{th} reactor with a nickel-based oxygen carrier. *Combust. Flame* **2010**, *157*, 934.
(41) Xiao, R.; Chen, L.; Saha, C.; Zhang, S.; Bhattacharya, S. Pressurized chemical-looping combustion of coal using an iron ore as oxygen carrier in a pilot-scale unit. *Int. J. Greenhouse Gas Control* **2012**, *10*, 363.
(42) Thon, A.; Kramp, M.; Hartge, E. U.; Heinrich, S.; Werther, J. Operational experience with a system of coupled fluidized beds for chemical looping combustion of solid fuels using ilmenite as oxygen carrier. *Appl. Energy* **2014**, *118*, 309.
(43) Markström, P.; Linderholm, C.; Lyngfelt, A. Operation of a 100 kW chemical-looping combustor with Mexican petroleum coke and Cerrejón coal. *Appl. Energy* **2014**, *113*, 1830.
(44) Adánez, J.; Abad, A.; Perez-Vega, R.; de Diego, L. F.; García-Labiano, F.; Gayán, P. Design and Operation of a Coal-fired 50 kW_{th} Chemical Looping Combustor. *Energy Procedia* **2014**, *63*, 63.
(45) Ma, J.; Zhao, H.; Tian, X.; Wei, Y.; Rajendran, S.; Zhang, Y.; Bhattacharya, S.; Zheng, C. Chemical looping combustion of coal in a 5 kW_{th} interconnected fluidized bed reactor using hematite as oxygen carrier. *Appl. Energy* **2015**, *157*, 304.
(46) Ströhle, J.; Orth, M.; Epple, B. Design and operation of a 1 MW_{th} chemical looping plant. *Appl. Energy* **2014**, *113*, 1490.
(47) Tong, A.; Bayham, S.; Kathe, M. V.; Zeng, L.; Luo, S.; Fan, L. Iron-based syngas chemical looping process and coal-direct chemical looping process development at Ohio State University. *Appl. Energy* **2014**, *113*, 1836.
(48) Luo, S.; Bayham, S.; Zeng, L.; McGiveron, O.; Chung, E.; Majumder, A.; Fan, L. S. Conversion of metallurgical coke and coal using a Coal Direct Chemical Looping (CDCL) moving bed reactor. *Appl. Energy* **2014**, *118*, 300.
(49) Bayham, S.; McGiveron, O.; Tong, A.; Chung, E.; Kathe, M.; Wang, D.; Zeng, L.; Fan, L. S. Parametric and dynamic studies of an iron-based 25-kW_{th} coal direct chemical looping unit using sub-bituminous coal. *Appl. Energy* **2015**, *145*, 354.
(50) Wang, X.; Liu, H.; Jin, B.; Zhao, J.; Sun, C.; Snape, C. E. Experimental Evaluation of a Chinese Sulfur-Containing Lean Iron Ore as the Oxygen Carrier for Chemical Looping Combustion. *Ind. Eng. Chem. Res.* **2016**, *55*, 428.
(51) Linderholm, C.; Schmitz, M.; Knutsson, P.; Källén, M.; Lyngfelt, A. Use of low-volatile solid fuels in a 100 kW chemical-looping combustor. *Energy Fuels* **2014**, *28*, 5942.
(52) Wang, X.; Jin, B.; Zhong, W.; Zhang, M.; Huang, Y.; Duan, F. Flow Behaviors in a High-Flux Circulating Fluidized Bed. *Int. J. Chem. React. Eng.* **2008**, *6*.10.2202/1542-6580.1780
(53) Issangya, A. S.; Bai, D.; Bi, H. T.; Lim, K. S.; Zhu, J.; Grace, J. R. Suspension densities in a high-density circulating fluidized bed riser. *Chem. Eng. Sci.* **1999**, *54*, 5451.
(54) Namkung, W.; Kim, S. W.; Kim, S. D. Flow regimes and axial pressure profiles in a circulating fluidized bed. *Chem. Eng. J.* **1999**, *72*, 245.
(55) Li, Z. Q.; Wu, C. N.; Wei, F.; Jin, Y. Experimental study of high-density gas-solids flow in a new coupled circulating fluidized bed. *Powder Technol.* **2004**, *139*, 214.
(56) Cuadrat, A.; Abad, A.; García-Labiano, F.; Gayán, P.; de Diego, L. F.; Adánez, J. The use of ilmenite as oxygen-carrier in a 500 W_{th} Chemical-Looping Coal Combustion unit. *Int. J. Greenhouse Gas Control* **2011**, *5*, 1630.
(57) Kolbitsch, P.; Pröll, T.; Hofbauer, H. Modeling of a 120 kW chemical looping combustion reactor system using a Ni-based oxygen carrier. *Chem. Eng. Sci.* **2009**, *64*, 99.

DOI: 10.1021/acs.iecr.6b03028
Ind. Eng. Chem. Res. 2016, 55, 11775−11784